

# QUIET-SR: Quantum Image Enhancement Transformer for Single Image Super-Resolution

Siddhant Dutta<sup>1</sup>, Nouhaila Innan<sup>2,3</sup>, Khadijeh Najafi<sup>4</sup>, Sadok Ben Yahia<sup>4,5</sup>, Muhammad Shafique<sup>2,3</sup>

<sup>1</sup>SVKM's Dwarkadas J. Sanghvi College of Engineering, India

<sup>2</sup>eBRAIN Lab, Division of Engineering, New York University Abu Dhabi (NYUAD), Abu Dhabi, UAE

<sup>3</sup>Center for Quantum and Topological Systems (CQTS), NYUAD Research Institute, NYUAD, Abu Dhabi, UAE

<sup>4</sup>The Maersk Mc-Kinney Moller Institute, University of Southern Denmark, Sønderborg, Denmark

<sup>5</sup>Department of Software Science, Tallinn University of Technology, Tallinn, Estonia

**Email:** forsomethingnewsid@gmail.com, nouhaila.innan@nyu.edu,  
sonaa.najafi@gmail.com, say@mmmi.sdu.dk, muhammad.shafique@nyu.edu

## Abstract

*Recent advancements in Single-Image Super-Resolution (SISR) using deep learning have significantly improved image restoration quality. However, the high computational cost of processing high-resolution images due to the large number of parameters in classical models, along with the scalability challenges of quantum algorithms for image processing, remains a major obstacle. In this paper, we propose the Quantum Image Enhancement Transformer for Super-Resolution (QUIET-SR), a hybrid framework that extends the Swin transformer architecture with a novel shifted quantum window attention mechanism, built upon variational quantum neural networks. QUIET-SR effectively captures complex residual mappings between low-resolution and high-resolution images, leveraging quantum attention mechanisms to enhance feature extraction and image restoration while requiring a minimal number of qubits, making it suitable for the Noisy Intermediate-Scale Quantum (NISQ) era. We evaluate our framework in MNIST (30.24 PSNR, 0.989 SSIM), FashionMNIST (29.76 PSNR, 0.976 SSIM) and the MedMNIST dataset collection, demonstrating that QUIET-SR achieves PSNR and SSIM scores comparable to state-of-the-art methods while using fewer parameters. These findings highlight the potential of scalable variational quantum machine learning models for SISR, marking a step toward practical quantum-enhanced image super-resolution.*

## 1. Introduction

Single-Image Super-Resolution (SISR) aims to recover a High-Resolution (HR) image from a Low-Resolution (LR)

input image [4]. Formally, given a low-resolution image  $I_{LR}$ , the objective of SISR is to reconstruct a high-resolution image  $I_{HR}$  such that the perceptual quality and structural fidelity of the resulting image closely approximate those of an ideal high-resolution reference. More formally, the original high-resolution image can be considered the ground truth, representing the scene sampled at a sufficiently high spatial resolution to capture fine details without degradation. In a physical sense, real-world scenes exist as continuous signals, and an ideal high-resolution image corresponds to a discretized representation with minimal loss of spatial information. The aim is to learn a mapping  $f : I_{LR} \rightarrow I_{HR}$  that reconstructs an image  $I_{HR}$  approximating this ideal ground truth. This technique has significant applications in fields such as medical imaging, satellite imagery, and autonomous driving as it helps enhance scans like MRIs, aiding in disease detection, improves the clarity of earth observation data for environmental monitoring and disaster response, and sharpens camera inputs, improving object recognition for safer navigation respectively. By recovering lost details, SISR enables better decision-making across these fields [11, 17, 22].

In the context of deep learning, traditional SISR methods often use Convolutional Neural Networks (CNNs) that incorporate residual learning, a technique that helps the network focus on reconstructing lost high-frequency details rather than relearning the entire image structure [9, 16]. Another common approach involves Generative Adversarial Networks (GANs), which generate high-resolution images by training two competing networks to improve image quality [14]. However, these methods are computationally demanding and struggle to scale efficiently as the size of the image and complexity increase. Recent developments in

SISR models, such as those based on Swin Transformer architectures, have demonstrated state-of-the-art performance in capturing fine details while maintaining contextual integrity, highlighting the ongoing demand for scalable and efficient approaches in this field [7, 15]. Quantum Computing (QC) introduces a representational-based computational paradigm that leverages quantum states to encode and manipulate high-dimensional data more efficiently. This approach has the potential to overcome certain limitations of classical computation in tasks requiring complex feature representations, such as extracting fine textures, spatial relationships, and high-frequency details in image processing [24]. Classical methods often struggle with the exponential growth of data, high memory and computational demands, and the difficulty of solving non-convex optimization problems, making quantum techniques a promising alternative for more scalable and efficient solutions. The field of Quantum Machine Learning (QML) utilizes the unique properties of quantum mechanics to investigate state spaces that are infeasible via classical approaches [3], to improve learning efficiency and model generalization. However, practical implementations of quantum image processing face challenges, primarily due to limitations in qubit resources and the presence of quantum noise [19, 24]. Current research in quantum Super-Resolution (SR) predominantly focuses on theoretical frameworks with limited practical implementations. This is largely due to the qubit requirements that exceed the capabilities of existing hardware [6, 21]. Several works have employed adiabatic QC with D-Wave systems, achieving proof-of-concept results [5].

In this paper, we tackle the dual challenge of leveraging Noisy Intermediate-Scale Quantum (NISQ) computers [18] while efficiently integrating QC with classical deep learning for super-resolution. A major obstacle is the inherent difficulty of combining quantum feature representations with classical deep learning models in a way that effectively utilizes the potential quantum advantages without being bottlenecked by hardware limitations. This challenge motivates our exploration of NISQ devices and the development of hybrid approaches that can overcome their constraints while achieving comparable or improved performance in SISR. To address this, we introduce a novel hybrid quantum-classical architecture for SISR. Our proof-of-concept framework demonstrates a scalable hybrid quantum super-resolution system, operating with fewer than 10 qubits per circuit within the proposed architecture. This represents a step toward practical quantum applications in image processing while staying within current quantum hardware constraints, as shown in Fig. 1. **The novel contributions of our work can be summarized as follows:**

1. We introduce QUIET-SR, a novel hybrid quantum-classical model that enhances image resolution. Our approach integrates a quantum-based attention mechanism

with a classical deep learning framework for image reconstruction. The quantum component helps efficiently capture important image features, while the classical deep network ensures high-quality output.

2. We demonstrate that Quantum Neural Networks (QNNs) can be effectively used for image super-resolution within current hardware constraints. Our model operates using fewer than 10 qubits per circuit, making it the first functional variational quantum approach that is feasible on today’s quantum devices.
3. We propose Shifted Quantum Window Attention (SQWIN), a novel quantum attention mechanism that processes images by dividing them into small, non-overlapping regions (fixed-size windows) and shifting them in a structured way to capture spatial relationships more effectively. Using quantum states to process these windows, SQWIN improves the ability of the model to capture fine image details while remaining scalable for near-term quantum hardware.

The rest of the paper is organized as follows, Sec. 2 reviews related work in deep learning-based and quantum-enhanced super-resolution; Sec. 3 presents the proposed QUIET-SR framework, detailing patch embedding, SQWIN, and complexity analysis; Sec. 4 describes the experimental setup, benchmarking models, and performance evaluation using PSNR and SSIM; Sec. 5 concludes with key findings, limitations, and future directions for hybrid quantum-classical approaches in image super-resolution.

## 2. Related Work

**Limitations of Quantum Computing in SISR and the Opportunity Gap:** The integration of QC into SISR is an emerging research area. One early approach recasts the sparse coding optimization problem as a Quadratic Unconstrained Binary Optimization (QUBO) problem [1], expressed as:

$$\min_{\mathbf{z} \in \{0,1\}^n} (\mathbf{z}^T \mathbf{Q} \mathbf{z} + \mathbf{c}^T \mathbf{z}), \quad (1)$$

where  $\mathbf{Q}$  is a matrix that encodes the interaction between candidate basis elements,  $\mathbf{z}$  is a binary vector representing the selection of these elements, and  $\mathbf{c}$  accounts for linear contributions. Preliminary experiments using D-Wave’s 5760-qubit quantum annealer have shown promise in solving these QUBO formulations, potentially enabling faster discovery of sparse representations that aid HR reconstruction [5]. However, no implementations have yet leveraged current NISQ quantum computers for image super-resolution, highlighting an opportunity gap and the need for techniques to make it feasible.

**Deep Learning Approaches in SISR:** The evolution of deep learning in SISR began with SRCNN, introduced by Dong et al. [9], which established the foundational CNN framework for super-resolution. This model operated in

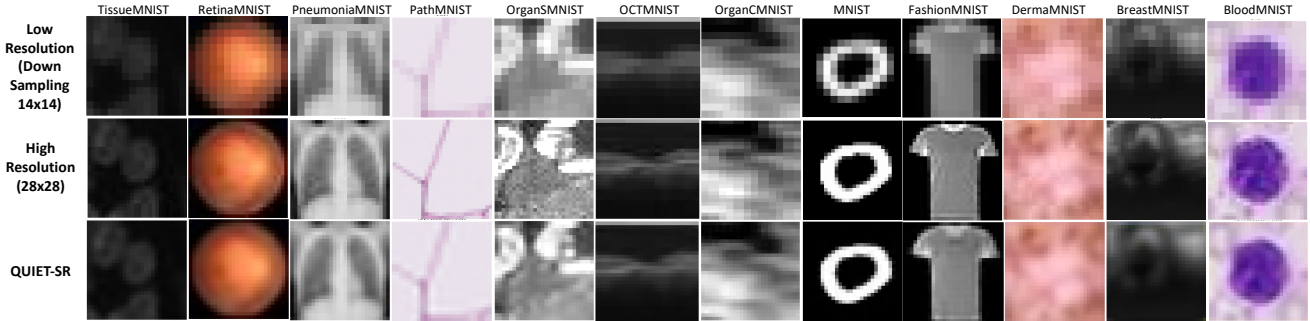


Figure 1. This grid compares low-resolution (14×14), high-resolution (28×28), and QUIET-SR super-resolution images across multiple MNIST-like datasets. The high-resolution row represents the ground truth, while the QUIET-SR row demonstrates the model’s capability to reconstruct fine details and preserve structural integrity. The super-resolved images generated by QUIET-SR closely approximate the high-resolution ground truth, effectively enhancing image clarity and preserving key features.

three key stages: patch extraction, where small overlapping regions of the low-resolution image were sampled as input; non-linear mapping, where a deep network learned complex transformations to infer high-resolution details; and reconstruction, where these enhanced patches were combined to generate the final high-resolution output. A major breakthrough came with SRGAN by Ledig *et al.* [14], which introduced GANs for SISR. By incorporating perceptual and adversarial loss functions, SRGAN focused on producing images with more realistic textures and finer details, moving beyond traditional pixel-wise optimization. Further advancements, such as EDSR [16] and RCAN [28], refined super-resolution by introducing enhanced residual learning and channel attention mechanisms, allowing deep networks to focus more effectively on key image features and improving their ability to learn complex high-resolution-to-low-resolution mappings.

**Sparse Approaches in SISR:** Sparse coding methods have provided a strong foundation for super-resolution, with Yang *et al.* [26] demonstrating the effectiveness of learning structured mappings between LR and HR image patches. Instead of directly mapping an LR patch to its HR counterpart, sparse coding represents each LR patch as a weighted combination of a small set of fundamental patterns (basis vectors), which are shared between the LR and HR domains. These sets of patterns, known as dictionaries, allow the model to reconstruct HR images using the same sparse representation  $\alpha$  found from the LR image. Mathematically, this is expressed as:

$$\mathbf{x} \approx \mathbf{D}_{\text{LR}}\alpha \quad \text{and} \quad \mathbf{y} \approx \mathbf{D}_{\text{HR}}\alpha, \quad (2)$$

where  $\mathbf{x}$  is the LR patch,  $\mathbf{y}$  is the reconstructed HR patch,  $\mathbf{D}_{\text{LR}}$  and  $\mathbf{D}_{\text{HR}}$  are the learned LR and HR dictionaries (i.e., sets of representative patterns), and  $\alpha$  is a sparse coefficient vector indicating which patterns are combined to approximate the image patch. The optimization problem for finding

the best  $\alpha$  is formulated as:

$$\min_{\alpha} \|\mathbf{x} - \mathbf{D}_{\text{LR}}\alpha\|_2^2 + \lambda\|\alpha\|_1, \quad (3)$$

where  $\lambda$  is a regularization parameter that encourages sparsity, ensuring that only a few basis vectors are selected for reconstruction. Timofte *et al.* [20] later improved upon this approach with anchored neighborhood regression, which combines local similarity-based regression with pre-computed global transformations. This method significantly speeds up computation by replacing the iterative sparse coding step with fast lookup-based matrix operations.

**Attention Mechanisms used in SISR:** Attention mechanisms have significantly advanced SISR by enabling models to selectively emphasize image features that are most relevant for reconstructing high-quality details at different scales. These mechanisms help the network focus on fine textures, edges, and structural patterns that are often lost in low-resolution images. One such approach is the Pixel Attention Network (PAN) by Zhao *et al.* [29], which introduces a method to dynamically adjust the importance of individual pixels based on their contribution to the overall image structure. This is achieved through an attention map, which assigns an adaptive weight to each pixel in the feature representation, determining how much influence it should have in the reconstruction process. Mathematically, this is represented by a three-dimensional matrix  $A \in \mathbb{R}^{C \times H \times W}$ , where  $C$  is the number of feature channels, and  $H$  and  $W$  are the spatial dimensions. The enhanced feature map  $x_k$  after applying pixel attention is given by:

$$x_k = f_{PA}(x_{k-1}) \cdot x_{k-1}, \quad (4)$$

where  $f_{PA}(\cdot)$  represents a  $1 \times 1$  convolution followed by a sigmoid activation function. This step refines the feature representation by selectively amplifying important pixel contributions and suppressing less informative ones.

Transformer-based architectures, such as the Swin Transformer [7, 15], build upon traditional attention mechanisms by organizing image information in a structured manner. Instead of analyzing the entire image at once, these models break it into smaller, non-overlapping regions, referred to as windows, and process them separately. To ensure the network still captures larger structures, the position of these windows is shifted in subsequent layers, allowing different parts of the image to be connected progressively. This hierarchical approach allows the model to first focus on high-frequency features within small regions before gradually integrating broader patterns across the entire image. By balancing local precision with a global understanding of the image, this method significantly improves reconstruction quality. However, these models often require a large number of parameters, which increases computational costs, motivating the exploration of alternative approaches that can achieve similar performance while reducing complexity.

### 3. Proposed Approach and Key Ideas

In this section, we present the design and implementation of QUIET-SR, a quantum image enhancement transformer for SISR as shown in Fig. 2. Our approach integrates quantum-enhanced attention mechanisms within a classical deep learning framework to efficiently reconstruct high-resolution images from low-resolution inputs. This section outlines the architecture of QUIET-SR, including the key quantum components and their role in image reconstruction.

**Variational Quantum Architecture.** QUIET-SR employs a variational/hybrid quantum-classical architecture for SISR as visually portrayed in Fig. 2. The quantum components appear in two specific areas: the MLP and the attention mechanism, which are replaced by Quantum MLP and quantum attention mechanism respectively. The remainder of the architecture maintains its classical nature, allowing for the utilization of classical computing’s data processing capabilities in image processing. There are key novel architectural implementations that highlight the improvements: (1) to address the scalability and quantum resource bottlenecks for generating high-quality super-resolution images, QUIET-SR utilizes classical patch embeddings by dividing the input image  $I$  into smaller non-overlapping patches  $P_i$ , and (2) to reduce parameterization caused by classical attention layers in the shifted window attention mechanism of Swin Transformer, we utilize a quantum attention mechanism which leverages the probabilistic states of qubits as queries, keys, and values within the Hilbert space to effectively capture the interrelated relationships within the pixel-wise information.

**Patch Embedding and Shallow Feature Extraction.** A key design decision in our framework stems from the limited number of qubits available, making it challenging to

process images as a whole. We address the limited number of qubits available by dividing the input image  $I$  into smaller non-overlapping patches  $P_i$ , where each patch is represented as:

$$P_i = I[h : h + p, w : w + p], \quad i \in \{1, 2, \dots, N\}, \quad (5)$$

where  $p \times p$  is the patch size,  $(h, w)$  represents the starting position of the patch, and  $N$  is the total number of patches. To extract shallow features, we apply a convolutional layer. Let  $F_{\text{shallow}}$  denote the feature map obtained after convolution. These extracted shallow features  $F_{\text{shallow}}$  retain low-frequency information [7] and serve as input for subsequent quantum attention mechanisms.

**Quantum Multi-layer Perceptron.** This architecture integrates quantum processing capabilities within a classical neural network framework to enhance feature representation and transformation. The QMLP extends traditional MLPs by incorporating a variational quantum circuit as a core computational element between classical linear transformations. The transformation process in QMLP can be formally expressed through a sequence of operations. The quantum processing layer employs a multi-basis rotation encoding scheme that varies depending on the depth of the quantum circuit. For deeper quantum circuits where the number of layers are more than 1, the system utilizes all three Pauli rotation gates ( $R_X$ ,  $R_Y$ , and  $R_Z$ ), while for shallow circuits where there is monolayer circuit, only  $R_Z$  rotations are applied. This adaptive approach can be formalized as:

$$\mathcal{R} = \begin{cases} \{R_X, R_Y, R_Z\}, & \text{if } L > 1, \\ \{R_Z\}, & \text{if } L = 1, \end{cases} \quad (6)$$

where  $N_L$  are the number of quantum layers.

For each rotation basis  $R \in \mathcal{R}$ , the input features  $\mathbf{h}_1$  are encoded into the quantum system through angle embedding:

$$S_R(\mathbf{h}_1) = \prod_{i=1}^n R(\phi_i(\mathbf{h}_1)), \quad (7)$$

where  $\phi_i(\mathbf{h}_1)$  represents the mapping of classical data to rotation angles for the  $i$ -th qubit, and  $R \in \{R_X, R_Y, R_Z\}$  corresponds to the rotation operators around the  $X$ ,  $Y$ , and  $Z$  axes respectively:

$$R(\hat{n}, \phi) = \begin{pmatrix} \cos(\phi/2) - i n_z \sin(\phi/2) & -i(n_x - i n_y) \sin(\phi/2) \\ -i(n_x + i n_y) \sin(\phi/2) & \cos(\phi/2) + i n_z \sin(\phi/2) \end{pmatrix}$$

, where  $\hat{n} = (n_x, n_y, n_z)$  is a unit vector defining the rotation axis, and  $\vec{\sigma} = (X, Y, Z)$  represents the Pauli matrices. Following each rotation encoding, an entangling layer is applied:

$$V(\theta) = \prod_{l=1}^L \left[ \prod_{i=1}^n R_{\phi}(\theta_{l,i}) \right] \left[ \prod_{i=1}^{n-1} \text{CNOT}_{i,i+1} \right], \quad (8)$$

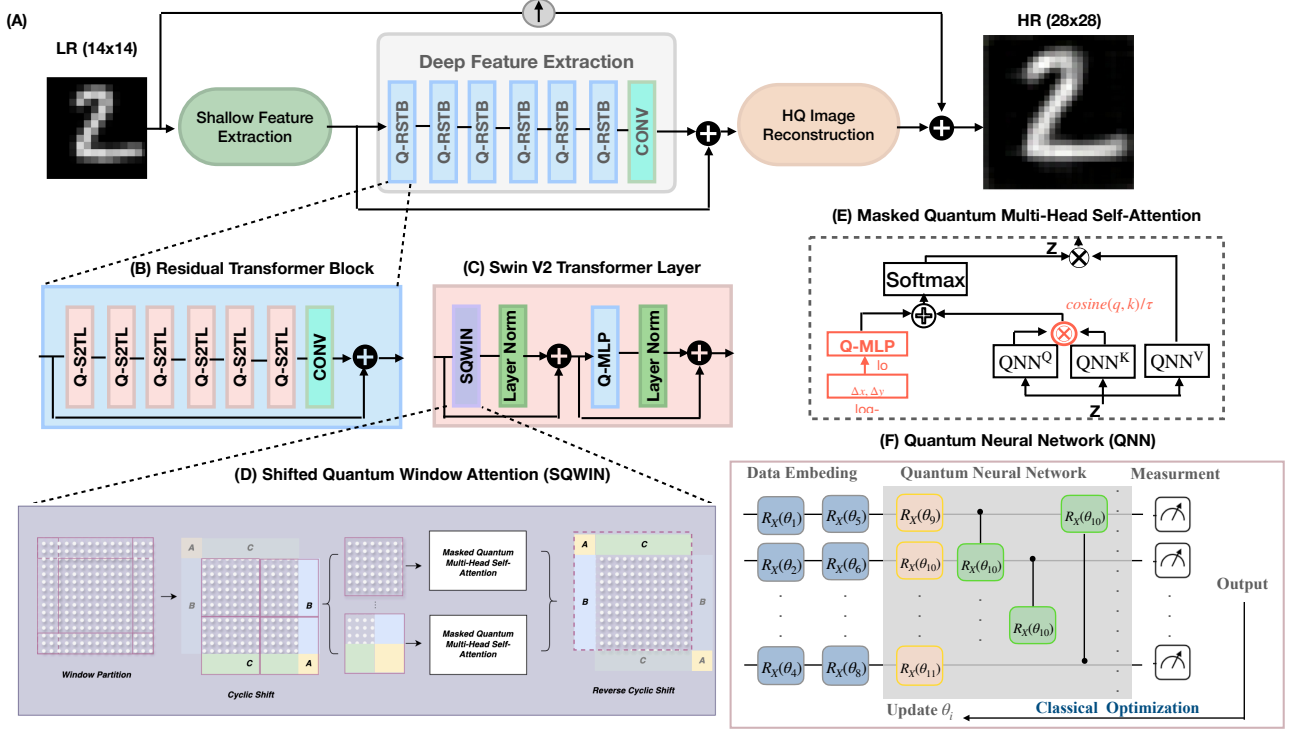


Figure 2. Architecture of the QUIET-SR framework, it comprises several stages designed to perform SISR efficiently. The pipeline initiates with patch embedding, where the LR input image is partitioned into patches and projected into a high-dimensional feature space. This step is followed by shallow feature extraction and deep feature extraction, which employ Residual Swin Transformer Blocks (RSTBs) and a residual transformer block with SwinV2 Transformer Layers (S2TL) for robust feature modeling. At the core of the architecture is the SQWIN mechanism, which incorporates QNNs to calculate queries (Q), keys (K), and values (V) for scaled dot-product attention. The QNN architecture uses angle embedding and basic entangler layers to transform features and optimize attention efficiency. The final stage, SR Image Reconstruction, synthesizes the SR output, demonstrating the advantages of quantum-enhanced image restoration.

where  $\text{CNOT}_{i,j}$  represents a controlled-NOT gate with qubit  $i$  as control and qubit  $j$  as target, enabling quantum entanglement between adjacent qubits. This entanglement operation is crucial for establishing non-local correlations that contribute to the quantum advantage in feature processing. The complete quantum state preparation combines these rotational encodings with entangling layers:

$$|\psi(\mathbf{h}_1, \boldsymbol{\theta})\rangle = \prod_{R \in \mathcal{R}} V(\boldsymbol{\theta}_R) S_R(\mathbf{h}_1) |0\rangle^{\otimes n}. \quad (9)$$

The measurement process extracts classical information from the quantum state through expectation values of appropriate observables. The choice of observables depends on the quantum circuit depth:

$$\mathcal{O} = \begin{cases} \{X_i, Y_i, Z_i\}_{i=1}^n, & \text{if } L > 1, \\ \{Z_i\}_{i=1}^n, & \text{if } L = 1, \end{cases} \quad (10)$$

where  $X_i$ ,  $Y_i$ , and  $Z_i$  represent the Pauli operators applied to the  $i$ -th qubit. The expectation values are computed as:

$$[\mathbf{h}_2]_j = \langle \psi(\mathbf{h}_1, \boldsymbol{\theta}) | \mathcal{O}_j | \psi(\mathbf{h}_1, \boldsymbol{\theta}) \rangle, \quad (11)$$

for each observable  $\mathcal{O}_j \in \mathcal{O}$ . This multi-basis rotation scheme provides several theoretical advantages. For deeper circuits, using all three rotation bases ( $X$ ,  $Y$ ,  $Z$ ) allows the quantum system to explore a more complete Hilbert space, enabling more complex transformations. For shallow circuits, focusing solely on  $Z$  rotations provides computational efficiency while still leveraging quantum effects for feature processing.

**Shifted Quantum Window Attention (SQWIN).** This mechanism combines principles of self-attention and quantum variational circuits [2] to process image features efficiently, as illustrated in the architecture shown in the subsection D of Fig. 2. The quantum state is initially prepared using the parameterized quantum circuit, where the state vector is defined as:

$$|\psi(\boldsymbol{\theta})\rangle = M(\boldsymbol{\theta}) |0\rangle^{\otimes n}, \quad (12)$$

where  $M(\boldsymbol{\theta})$  represents the parameterized quantum circuit, and  $n$  denotes the number of qubits. The quantum circuit consists of sequential layers, where each layer involves rotation gates  $R_X(\theta_{i,i})$  applied to each qubit, followed by

---

**Algorithm 1: QUIET-SR**

---

**Input:** Low-resolution image  $I_{LR} \in \mathbb{R}^{H \times W \times C}$ , Upscaling factor  $s$ , Window size  $M$ , Number of quantum layers  $L$

**Output:** High-resolution image  $I_{HR} \in \mathbb{R}^{sH \times sW \times C}$

**Shallow Feature Extraction:**

$F_0 \leftarrow \text{Conv}_{3 \times 3}(I_{LR})$

**Function** QuantumLayer ( $x, \theta$ ):

Initialize PennyLane quantum circuit with  $n$  qubits  
Encode input  $x$  into quantum state using rotational embeddings  
Apply parameterized quantum layers with trainable weights  $\theta$   
Measure expectation values:  $\langle Z_i \rangle$  for  $i \in [1, n]$   
**return**  $[\langle Z_1 \rangle, \dots, \langle Z_n \rangle]$

**Function** ShiftedQuantumWindowAttention ( $X \in \mathbb{R}^{B \times N \times D}$ ,  $\text{shift\_size}$ ):

Partition input into windows:  $\{W_i\}_{i=1}^{N_w}$  of size  $M \times M$   
**if**  $\text{shift\_size} > 0$  **then**  
    Apply circular shift:  $X_{\text{shifted}} \leftarrow \text{Roll}(X, \text{shifts} = (-\text{shift\_size}, -\text{shift\_size}))$   
**else**  
     $X_{\text{shifted}} \leftarrow X$   
**foreach**  $W_i$  **do**  
     $QKV_i \leftarrow \text{QuantumLayer}(W_i * 3, \theta_{QKV})$   
    Compute quantum-enhanced attention:  
         $A_i \leftarrow \frac{Q_i K_i^T}{\sqrt{d}} + B$ , where  $B$  is the relative position bias  
    Apply softmax:  $A_i \leftarrow \text{softmax}(A_i)$   
    Compute output projection:  $O_i \leftarrow A_i V_i$   
    Apply final QuantumLayer:  
         $O_i \leftarrow \text{QuantumLayer}(O_i, \theta_O)$   
**if**  $\text{shift\_size} > 0$  **then**  
    Reverse the shift:  
         $O_{\text{final}} \leftarrow \text{Roll}(O, \text{shifts} = (\text{shift\_size}, \text{shift\_size}))$   
**return**  $O_{\text{final}}$

**Main Network Forward Pass:**

**for**  $l \leftarrow 1$  **to**  $L$  **do**

**Quantum Swin Transformer Block:**

$X_l \leftarrow \text{LayerNorm}(F_{l-1})$   
 $A_l \leftarrow \text{ShiftedQuantumWindowAttention}(X_l, \text{shift\_size} = l \bmod 2 \times M/2)$   
 $F'_l \leftarrow F_{l-1} + \text{DropPath}(A_l)$

**Quantum MLP Block:**

$Y_l \leftarrow \text{LayerNorm}(F'_l)$   
 $M_l \leftarrow \text{QuantumLayer}(\text{MLP}(Y_l), \theta_{MLP})$   
 $F_l \leftarrow F'_l + \text{DropPath}(M_l)$

**Upsampling:**

$F_{\text{up}} \leftarrow \text{PixelShuffle}(\text{Conv}_{3 \times 3}(F_L))$   
 $I_{HR} \leftarrow \text{Conv}_{3 \times 3}(F_{\text{up}})$   
**return**  $I_{HR}$

---

entangling operations using controlled-NOT (CNOT) gates between consecutive qubits. The full circuit is described by  $V(\theta)$ , where  $L$  is the number of layers, and the combination of  $R_X(\theta_{l,i}) = e^{-i\theta_{l,i}X}$  and CNOT gates enables the generation of entangled quantum states that are crucial for capturing complex features in images. Our implementation utilizes a QuantumLayer consisting of rotational embeddings followed by entangling operations. The quantum attention mechanism employs cosine similarity with a learnable tem-

perature parameter to compute attention weights, which is then applied in the quantum domain to model interactions between image patches.

$$\text{Attn}(qkv) = \text{softmax}(\kappa \cdot \cos(qkv) + B_{\text{rel}}), \quad (13)$$

where  $\kappa$  is a learnable parameter that controls the attention logits and  $B_{\text{rel}}$  represents the relative position bias. This bias is computed through a continuous MLP-based approach  $B_{\text{rel}} = \text{QMLP}(R_{\text{table}})$  where  $R_{\text{table}}$  contains the normalized relative position coordinates transformed using a logarithmic encoding. These coordinates are scaled and processed through a two-layer MLP to generate head-specific positional biases. This quantum formulation of cosine attention ensures that the relationships between image patches are effectively captured, enabling the recovery of high-resolution details in the image. The final output is computed, where a second quantum transformation is applied to the weighted combination of values. This dual quantum processing enables the model to better capture non-local dependencies and complex feature relationships, enhancing the recovery of high-resolution details in images.

**Quantum Resource Estimation of QUIET-SR.** For each quantum layer in the QUIET-SR model, the resource requirements are determined by the number of qubits needed to encode the quantum states and any additional ancilla qubits required for the quantum circuit implementation  $\lceil \log_2(D) \rceil + a$ , where  $\lceil \log_2(D) \rceil$  represents the number of qubits required to encode the  $D$ -dimensional quantum state, where  $D$  is the embedding dimension. The term  $a$  denotes the additional ancilla qubits necessary to facilitate the quantum computation, such as those used for error correction or intermediate calculations. The quantum circuit depth scales as  $\mathcal{O}(D \log D)$  due to the quantum attention mechanism, which involves operations that grow logarithmically with respect to  $D$ . This scaling arises from the quantum attention mechanism, where the quantum states interact and produce results that depend on these quantum dimensions. The quantum state preparation itself is represented as a linear combination of quantum basis states  $|\psi(x)\rangle = \sum_{i=0}^{D-1} \alpha_i |i\rangle$  where  $\alpha_i$  are the normalized feature values extracted from the input features. The relative position bias term  $B$  is computed using a combination of learned positional encoding terms:

$$B_{i,j} = \text{QMLP}(\log_2(1 + |\Delta x|/\gamma_x) \oplus \log_2(1 + |\Delta y|/\gamma_y)),$$

where  $\Delta x$  and  $\Delta y$  represent the differences in positions between elements, and  $\gamma_x$  and  $\gamma_y$  are learnable parameters. These terms contribute to capturing positional relationships between features, improving the attention mechanism.

## 4. Experiments and Results

In this section, we go over the results of QUIET-SR and provide an analysis of the key elements of the design.

Table 1. Quantitative comparisons of PSNR/SSIM across six complicated medical image datasets for an embedding dimension equal to the number of qubits (4). The best values among our models are highlighted in bold green, while the closest best values from current standard SOTA models are highlighted in a lighter green (Part 1).

Method	BloodMNIST		BreastMNIST		DermaMNIST		OCTMNIST		OrganCMNIST		OrganSMNIST	
	PSNR	SSIM	PSNR	SSIM	PSNR	SSIM	PSNR	SSIM	PSNR	SSIM	PSNR	SSIM
Nearest Neighbor	18.35	0.748	16.46	0.689	20.35	0.812	19.35	0.792	12.95	0.594	12.93	0.611
Bilinear	19.87	0.772	17.98	0.712	21.97	0.834	20.83	0.816	14.38	0.625	14.35	0.642
Bicubic	21.63	0.812	19.71	0.752	22.72	0.867	22.58	0.848	16.14	0.662	16.08	0.683
Sparse Representation	22.15	0.836	20.23	0.776	22.84	0.891	22.81	0.874	17.69	0.683	17.63	0.705
Iterative Back-projection	22.68	0.861	21.75	0.799	22.96	0.913	22.94	0.896	19.24	0.709	19.18	0.731
SRCNN	29.20	0.896	26.27	0.832	36.28	0.941	31.17	0.928	20.79	0.742	20.73	0.764
Swin2SR	30.42	0.932	27.49	0.872	37.55	0.961	32.44	0.949	21.93	0.768	21.89	0.792
<b>QUIET-SR (ours)</b>	<b>31.24</b>	<b>0.950</b>	<b>28.35</b>	<b>0.894</b>	<b>38.24</b>	<b>0.973</b>	<b>33.24</b>	<b>0.963</b>	<b>22.80</b>	<b>0.814</b>	<b>22.81</b>	<b>0.811</b>

Table 2. Quantitative comparisons of PSNR/SSIM across six datasets from digits, fashion, and medical categories for an embedding dimension equal to the number of qubits (4). The best values among our models are highlighted in bold green, while the closest best values from current SOTA models are highlighted in a lighter green (Part 2).

Method	PathMNIST		PneumoniaMNIST		RetinaMNIST		FashionMNIST		MNIST		TissueMNIST	
	PSNR	SSIM	PSNR	SSIM	PSNR	SSIM	PSNR	SSIM	PSNR	SSIM	PSNR	SSIM
Nearest Neighbor	16.87	0.620	18.82	0.775	19.98	0.777	16.83	0.776	17.32	0.789	21.18	0.775
Bilinear	18.39	0.651	20.34	0.806	21.50	0.808	18.35	0.807	18.84	0.820	22.70	0.806
Bicubic	20.15	0.692	21.11	0.846	22.27	0.848	20.11	0.847	20.60	0.859	22.86	0.846
Sparse Representation	21.67	0.721	22.63	0.876	22.79	0.878	21.63	0.877	22.12	0.889	22.93	0.876
Iterative Back-projection	22.19	0.751	22.75	0.906	22.86	0.908	22.15	0.907	22.64	0.919	22.98	0.906
SRCNN	26.71	0.781	30.67	0.935	31.83	0.937	27.67	0.936	28.16	0.949	35.02	0.935
Swin2SR	27.93	0.805	31.89	0.954	33.05	0.956	28.89	0.960	29.38	0.972	36.29	0.954
<b>QUIET-SR (ours)</b>	<b>28.82</b>	<b>0.820</b>	<b>32.73</b>	<b>0.966</b>	<b>33.91</b>	<b>0.967</b>	<b>29.76</b>	<b>0.976</b>	<b>30.24</b>	<b>0.989</b>	<b>37.12</b>	<b>0.966</b>

**Datasets.** QUIET-SR is evaluated on MNIST and 12 additional datasets from the MNIST-like family, covering both general and medical imaging domains. To introduce additional complexity, the model is trained on the full dataset without prior knowledge of class information, ensuring generalization without explicit supervision. High-resolution images are downsampled by a factor of 2 to produce low-resolution counterparts with dimensions of  $14 \times 14$ , following standard super-resolution benchmarks. Our evaluation utilizes diverse datasets including MNIST (handwritten digits) [8], FashionMNIST (clothing/accessories) [25], and medical imaging collections [27] spanning BloodMNIST (healthy blood cells), BreastMNIST (ultrasounds), DermaMNIST (skin lesions), OCTMNIST (retinal images), OrganSMNIST/CMNIST (liver tumor CT scans), PathMNIST (colorectal cancer histology), PneumoniaMNIST (chest X-rays), RetinaMNIST (fundus images), and TissueMNIST (human tissue histology) to thoroughly assess performance across standard and specialized domains.

**Training Setup.** The QUIET-SR architecture consists of six layers, each with a window size of 2, an embedding dimension of 4, and 4 attention heads. A *QMLP* with a ratio of 2 is used to refine feature representations. The

pixel shuffle technique, specifically the auxiliary variant, is employed for upsampling, ensuring efficient reconstruction of fine details. The model is trained using the Adam optimizer [12] with a learning rate of  $2 \times 10^{-4}$ , and the  $L_1$  loss function [10], also known as Mean Absolute Error (MAE), is used to minimize the pixel-wise reconstruction error between the super-resolved image  $I_{SR}$  and the ground truth high-resolution image  $I_{HR}$ . It is defined as:

$$L_1 = \frac{1}{N} \sum_{i=1}^N |I_{SR}[i] - I_{HR}[i]|, \quad (14)$$

where  $N$  represents the total number of pixels in the image. This loss function penalizes the absolute differences between the predicted and ground truth pixel values, encouraging sharp and accurate reconstructions. Training is conducted for 25 epochs with a batch size of 64, utilizing Ampere GPU acceleration to expedite computation.

**Metrics & Benchmarking Models.** The quality of the reconstructed images is evaluated using two widely adopted metrics: Peak Signal-to-Noise Ratio (PSNR) [13] and Structural Similarity Index Measure (SSIM) [23]. These metrics quantitatively assess the fidelity of the super-resolved images relative to the ground truth. PSNR mea-

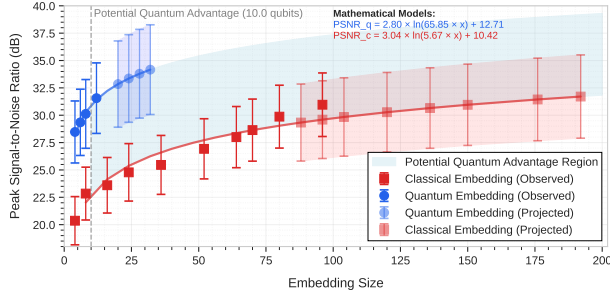


Figure 3. This comparative analysis illustrates the relationship between embedding dimension (number of qubits in quantum systems) and PSNR. Empirical measurements (solid lines) are shown for both quantum and classical embeddings up to 10 qubits, beyond which projections (dashed lines) are generated using a logarithmic regression model. The shaded region represents the predicted performance advantage of QUIET-SR quantum embeddings over their classical counterparts as quantum hardware capabilities expand. The diverging trajectories suggest that quantum embeddings may offer increasingly significant advantages in image reconstruction quality as larger quantum systems become available, with the performance gap widening in proportion to system size.

sures the logarithmic ratio between the maximum possible signal value and the distortion introduced by reconstruction errors. SSIM quantifies the structural similarity between the super-resolved and ground truth images by considering luminance, contrast, and structure. Higher PSNR & SSIM values correspond to better reconstruction quality. The benchmarking results can be seen in Tables 1 and 2.

**QUIET-SR Key Results and SOTA Comparison.** The quantitative evaluation suggests that QUIET-SR demonstrates improved performance metrics compared to conventional approaches, with enhanced PSNR indicating reduced pixel-wise reconstruction errors and higher SSIM values suggesting better preservation of structural information in the reconstructed images as shown in Fig. 1. As evidenced in the Tables 1 and 2, conventional interpolation techniques yield comparatively lower scores due to their limited capacity to reconstruct fine details, while bicubic interpolation shows only marginal improvements but exhibits limitations in preserving complex textural information. Methods employing iterative back-projection and sparse representation demonstrate incremental improvements through frequency-domain analysis and iterative refinement processes; however, their performance metrics remain below those achieved by deep learning architectures, with SR-CNN achieving improved metrics through hierarchical feature learning despite being constrained by architectural depth limitations, and Swin2SR showing notable improvement through its capacity to model long-range dependencies and contextual information, yet comparative analysis indicates that QUIET-SR consistently produces superior re-

sults across the evaluated datasets while maintaining a relatively efficient model size of 1.55MB, potentially making it suitable for deployment in environments with computational constraints, with its apparent capacity to preserve structural details being particularly relevant for specialized applications in medical imaging, where reconstruction fidelity can influence diagnostic accuracy and pattern recognition tasks.

**Why Does QUIET-SR Work Effectively?** *Effect of Quantum Attention Mechanism.* Recalling that QUIET-SR employs a high representational rich embedding feature space provided by the quantum attention mechanism with the goal to effectively capture features that can output a high resolution image from a low resolution input, the comparative analyses in Tables 1 and 2 offer further insights into its efficacy. The observed performance improvements can be attributed to the quantum attention mechanism’s ability to exploit non-local correlations and capture complex, high-dimensional feature interactions. This is achieved through an adaptive embedding strategy that harnesses multiple rotation bases and entanglement operations, enabling a more discriminative and context-aware representation. Consequently, QUIET-SR is able to preserve fine structural details and achieve superior reconstruction quality across varying imaging scenarios, a result that substantiates its potential in addressing the challenges inherent in super-resolution tasks for medical images.

**QUIET-SR Resource Efficiency and Embedding Dimension Scaling on NISQ-Era Quantum Machines.** As demonstrated in Fig. 3, QUIET-SR’s performance improvements underscore its scalability on current NISQ quantum machines. Despite qubits remaining a scarce resource in the NISQ era, the distributed architecture of QUIET-SR’s quantum circuits enables efficient resource allocation. This design facilitates parallel execution of multiple circuits, allowing scaling to larger embedding dimensions even with limited qubit availability. The performance curve indicates that even modest increases in embedding size yield noticeable gains in PSNR, reflecting improved recovery of high-resolution details. This behavior demonstrates that the variational quantum circuits within QUIET-SR capture complex, non-local features in image data that traditional methods might overlook. As a result, QUIET-SR establishes itself as the first variational image super-resolution algorithm leveraging distributed quantum processing—efficiently utilizing limited qubit resources while establishing a promising direction for future developments as quantum hardware advances.

## 5. Conclusion

QUIET-SR is the first hybrid quantum-classical framework that demonstrates the practical potential of QC in image processing applications within current hardware



constraints. By successfully implementing a quantum-enhanced super-resolution system that operates within a limited qubit environment constraint per circuit, we have shown that meaningful quantum advantages can be achieved even with NISQ devices.

## Acknowledgments

This work was supported in part by the NYUAD Center for Quantum and Topological Systems (CQTS), funded by Tamkeen under the NYUAD Research Institute grant CG008.

## References

- [1] Md Zahangir Alom, Brian Van Essen, Adam T. Moody, David Peter Widemann, and Tarek M. Taha. Quadratic unconstrained binary optimization (qubo) on neuromorphic computing system. In *2017 International Joint Conference on Neural Networks (IJCNN)*, pages 3922–3929, 2017. 2
- [2] Marcello Benedetti, Erika Lloyd, Stefan Sack, and Mattia Fiorentini. Parameterized quantum circuits as machine learning models. *Quantum Science and Technology*, 4(4):043001, 2019. 5
- [3] Jacob Biamonte, Peter Wittek, Nicola Pancotti, Patrick Rebentrost, Nathan Wiebe, and Seth Lloyd. Quantum machine learning. *Nature*, 549(7671):195–202, 2017. 2
- [4] Qizhou Chen and Qing Shao. Single image super-resolution based on trainable feature matching attention network. *Pattern Recognition*, 149:110289, 2024. 1
- [5] Han Yao Choong, Suryansh Kumar, and Luc Van Gool. Quantum annealing for single image super-resolution. In *Proceedings of the IEEE/CVF Conference on Computer Vision and Pattern Recognition*, pages 1150–1159, 2023. 2
- [6] Marçal Comajoan Cara, Gopal Ramesh Dahale, Zhongtian Dong, Roy T Forestano, Sergei Gleyzer, Daniel Justice, Kyoungchul Kong, Tom Magorsch, Konstantin T Matchev, Katia Matcheva, et al. Quantum vision transformers for quark-gluon classification. *Axioms*, 13(5):323, 2024. 2
- [7] Marcos V Conde, Ui-Jin Choi, Maxime Burchi, and Radu Timofte. Swin2sr: Swinv2 transformer for compressed image super-resolution and restoration. In *European Conference on Computer Vision*, pages 669–687. Springer, 2022. 2, 4
- [8] Li Deng. The mnist database of handwritten digit images for machine learning research. *IEEE Signal Processing Magazine*, 29(6):141–142, 2012. 7
- [9] Chao Dong, Chen Change Loy, Kaiming He, and Xiaoou Tang. Image super-resolution using deep convolutional networks. *IEEE transactions on pattern analysis and machine intelligence*, 38(2):295–307, 2015. 1, 2
- [10] Xiangyu He and Jian Cheng. Revisiting l1 loss in super-resolution: a probabilistic view and beyond. *arXiv preprint arXiv:2201.10084*, 2022. 7
- [11] Jithin Saji Isaac and Ramesh Kulkarni. Super resolution techniques for medical image processing. In *2015 International Conference on Technologies for Sustainable Development (ICTSD)*, pages 1–6, 2015. 1
- [12] Diederik P Kingma. Adam: A method for stochastic optimization. *arXiv preprint arXiv:1412.6980*, 2014. 7
- [13] Jari Korhonen and Junyong You. Peak signal-to-noise ratio revisited: Is simple beautiful? In *2012 Fourth International Workshop on Quality of Multimedia Experience*, pages 37–38, 2012. 7
- [14] Christian Ledig, Lucas Theis, Ferenc Huszár, Jose Caballero, Andrew Cunningham, Alejandro Acosta, Andrew Aitken, Alykhan Tejani, Johannes Totz, Zehan Wang, et al. Photo-realistic single image super-resolution using a generative adversarial network. In *Proceedings of the IEEE conference on computer vision and pattern recognition*, pages 4681–4690, 2017. 1, 3
- [15] Jingyun Liang, Jiezhong Cao, Guolei Sun, Kai Zhang, Luc Van Gool, and Radu Timofte. Swinir: Image restoration using swin transformer. In *Proceedings of the IEEE/CVF international conference on computer vision*, pages 1833–1844, 2021. 2, 4
- [16] Bee Lim, Sanghyun Son, Heewon Kim, Seungjun Nah, and Kyoung Mu Lee. Enhanced deep residual networks for single image super-resolution. In *Proceedings of the IEEE conference on computer vision and pattern recognition workshops*, pages 136–144, 2017. 1, 3
- [17] Krzysztof Okarma, Mateusz Teclaw, and Piotr Lech. Application of super-resolution algorithms for the navigation of autonomous mobile robots. In *Image Processing & Communications Challenges 6*, pages 145–152, Cham, 2015. Springer International Publishing. 1
- [18] John Preskill. Quantum computing in the nisq era and beyond. *Quantum*, 2:79, 2018. 2
- [19] Arsenii Senokosov, Alexandr Sedykh, Asel Saginalieva, Basil Kyriacou, and Alexey Melnikov. Quantum machine learning for image classification. *Machine Learning: Science and Technology*, 5(1):015040, 2024. 2
- [20] Radu Timofte, Vincent De, and Luc Van Gool. Anchored neighborhood regression for fast example-based super-resolution. In *2013 IEEE International Conference on Computer Vision*, pages 1920–1927, 2013. 3
- [21] Eyup B Unlu, Marçal Comajoan Cara, Gopal Ramesh Dahale, Zhongtian Dong, Roy T Forestano, Sergei Gleyzer, Daniel Justice, Kyoungchul Kong, Tom Magorsch, Konstantin T Matchev, et al. Hybrid quantum vision transformers for event classification in high energy physics. *Axioms*, 13(3):187, 2024. 2
- [22] Xuan Wang, Jinglei Yi, Jian Guo, Yongchao Song, Jun Lyu, Jindong Xu, Weiqing Yan, Jindong Zhao, Qing Cai, and Haigen Min. A review of image super-resolution approaches based on deep learning and applications in remote sensing. *Remote Sensing*, 14(21), 2022. 1
- [23] Zhou Wang, A.C. Bovik, H.R. Sheikh, and E.P. Simoncelli. Image quality assessment: from error visibility to structural similarity. *IEEE Transactions on Image Processing*, 13(4): 600–612, 2004. 7
- [24] Zhaobin Wang, Minzhe Xu, and Yaonan Zhang. Review of quantum image processing. *Archives of Computational Methods in Engineering*, 29(2):737–761, 2022. 2
- [25] Han Xiao, Kashif Rasul, and Roland Vollgraf. Fashion-mnist: a novel image dataset for benchmarking machine

learning algorithms. *arXiv preprint arXiv:1708.07747*, 2017.

7

- [26] Jianchao Yang, John Wright, Thomas Huang, and Yi Ma. Image super-resolution as sparse representation of raw image patches. In *2008 IEEE Conference on Computer Vision and Pattern Recognition*, pages 1–8, 2008. 3
- [27] Jiancheng Yang, Rui Shi, Donglai Wei, Zequan Liu, Lin Zhao, Bilian Ke, Hanspeter Pfister, and Bingbing Ni. Medmnist v2-a large-scale lightweight benchmark for 2d and 3d biomedical image classification. *Scientific Data*, 10(1):41, 2023. 7
- [28] Yulun Zhang, Kunpeng Li, Kai Li, Lichen Wang, Bineng Zhong, and Yun Fu. Image super-resolution using very deep residual channel attention networks. In *Proceedings of the European conference on computer vision (ECCV)*, pages 286–301, 2018. 3
- [29] Hengyuan Zhao, Xiangtao Kong, Jingwen He, Yu Qiao, and Chao Dong. Efficient image super-resolution using pixel attention. In *Computer Vision–ECCV 2020 Workshops: Glasgow, UK, August 23–28, 2020, Proceedings, Part III 16*, pages 56–72. Springer, 2020. 3